

Nanoscale

Accepted Manuscript



This is an *Accepted Manuscript*, which has been through the Royal Society of Chemistry peer review process and has been accepted for publication.

Accepted Manuscripts are published online shortly after acceptance, before technical editing, formatting and proof reading. Using this free service, authors can make their results available to the community, in citable form, before we publish the edited article. We will replace this *Accepted Manuscript* with the edited and formatted *Advance Article* as soon as it is available.

You can find more information about *Accepted Manuscripts* in the [Information for Authors](#).

Please note that technical editing may introduce minor changes to the text and/or graphics, which may alter content. The journal's standard [Terms & Conditions](#) and the [Ethical guidelines](#) still apply. In no event shall the Royal Society of Chemistry be held responsible for any errors or omissions in this *Accepted Manuscript* or any consequences arising from the use of any information it contains.

Cite this: DOI: 10.1039/c0xx00000x

www.rsc.org/xxxxxx

Metallic-nanowire-loaded silicon-on-insulator structures: a route to low-loss plasmon waveguiding on the nanoscale

Yusheng Bian^a and Qihuang Gong^{* a,b}

Received (in XXX, XXX) Xth XXXXXXXXXX 20XX, Accepted Xth XXXXXXXXXX 20XX

DOI: 10.1039/b000000x

The simultaneous realization of nanoscale field localization and low transmission loss remains one of the major challenges in nanophotonics. Metal nanowire waveguides can fulfill this goal to a certain extent by confining light within a subwavelength space, yet their optical performances are still restricted by the tradeoff between confinement and loss, which result in quite limited propagation distances when their mode sizes are reduced down to the nanometer scale. Here we introduce a class of low-loss guiding schemes by integrating silicon-on-insulator (SOI) waveguides with plasmon nanowire structures. The closely spaced silicon and metal configurations allow efficient light squeezing within the nanometer, low-index silica gaps between them, enabling deep-subwavelength light transmission with low modal attenuation. Optimizations of key structural parameters unravel the wide-range existence nature of the high-performance hybrid nanowire plasmon mode, which demonstrates improved guiding properties over the conventional hybrid and nanowire plasmon polaritons. Excitation strategy of the guided mode and the feasibility of the waveguide for compact photonic integrations as well as active components are also discussed to lay the foundations for its practical implementations. The remarkable properties of these metallic-nanowire-loaded SOI waveguides potentially lend themselves to the implementations of high performance nanophotonic components, and open up promising opportunities for a variety of intriguing applications on the nanoscale.

1. Introduction

Metallic nanowires are considered as ideal candidates for miniaturized integrated components and circuits, having found a wide range of intriguing applications in advanced photonic systems¹. As subwavelength information carriers, metal nanowire structures can support tightly confined surface plasmon polaritons (SPPs), thus allowing efficient squeezing of the optical mode size down to the subwavelength scale far beyond the diffraction limit². Compared with many other SPP guiding configurations³, these nanowire plasmonic waveguides have received increasing attention in recent years due to their simplicity in nature, remarkable optoelectronic properties and compatibility with a wide variety of synthetic methods. Numerous high-performance nanowire-based nanophotonic devices, including directional couplers⁴, logic gates⁵, resonators⁶ and nanolasers⁷, have also been demonstrated.

For a typical metal nanowire embedded in a homogenous dielectric material, the fundamental plasmonic mode (known as the TM₀ mode) exhibits rather weak field confinement for relatively large nanowire radius, while demonstrating strong localization around the nanowire interface when its geometric

size is reduced down to the sub-wavelength scale. A sacrifice associated with such sub-diffraction-limited mode confinement is the relatively large Ohmic loss, which results in quite limited propagation distance. The loss problem is further exacerbated when both the physical dimension of the nanowire and its mode size are squeezed into a deep-subwavelength scale, which hinders the further implementation of many practical applications. Despite significant efforts devoted to nanowire waveguides and modified guiding structures in recent years, including various schemes based on substrate-mediated guiding of nanowire plasmonic modes⁸⁻¹², the optical performances of these nanowire waveguides are still severely restricted by the tradeoff between confinement and loss. In particular, when the metallic nanowire is brought in close vicinity to a high-index dielectric substrate, dramatically shortened propagation distance due to the leakage radiation into the substrate would pose a great challenge for the implementation of high-performance light guiding using these metallic nanowire structures.

To overcome the limitations of single-dielectric-layer mediated plasmon waveguiding, hybrid configurations that integrate finitely thick silicon waveguides with crystallize metallic nanowires are recently proposed and theoretically studied by

Zhang et al.¹³. These waveguides not only offer improved balance between confinement and loss over the conventional nanowire-based plasmon structures, but also provide high compatibility with modern semiconductor fabrication strategies, thereby potentially lending themselves to a variety of practical applications. Although the guiding properties of metal nanowires sitting directly on thin silicon waveguides have been studied in¹³, a more general waveguide configuration that incorporates an additional buffer layer between the metal nanowire and the high-index dielectric layer has not yet been reported and systematically investigated so far. Moreover, detailed comparisons of such a structure with traditional nanowire and hybrid plasmonic waveguides, along with practical issues like waveguide crosstalk and feasibility for active components have yet to be explored. To address these issues, here we conduct comprehensive investigations on the characteristics of these metallic-nanowire-loaded SOI waveguides at telecommunication wavelengths. In addition to revealing their capabilities for low-loss light transport at the nanoscale, we also confirm that these waveguides not only feature low crosstalk, but also can be implemented as loss-less subwavelength guiding schemes when appropriate gain is introduced in low/high-index dielectric materials. Our studies are expected to pave the way for their potential applications in high-performance passive and active photonic components.

2. Metallic-nanowire-loaded SOI structures for nanoscale light transport: Studies on guided mode's properties

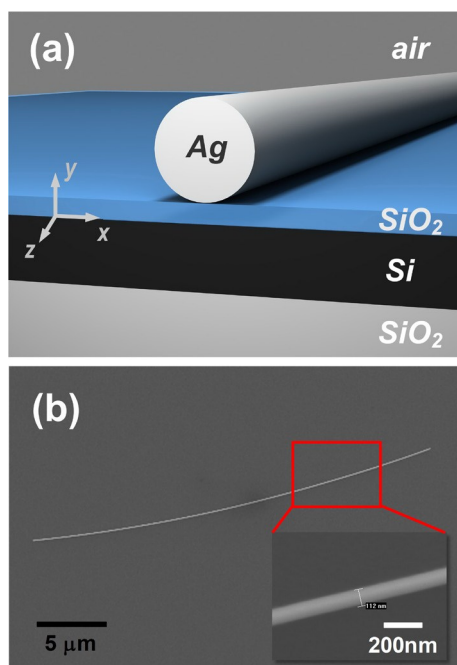


Fig.1 Metallic-nanowire-loaded SOI waveguide. (a) Sketch of the three-dimensional (3D) geometry, which is composed by a silver nanowire (with a radius of r and a refractive index of n_m) sitting above an infinitely wide, but finitely thick silicon waveguide (with a thickness of t and a refractive index of n_d) over a silica substrate (with a refractive index of n_s). The silica gap layer between the silicon waveguide and the silver nanowire has a thickness of g and a refractive index of n_g . The upper cladding is assumed to be air (refractive index n_c). (b) Scanning electron

microscope (SEM) image of a chemically synthesized silver nanowire on a silicon substrate (i.e., $g = 0$ nm, $t \rightarrow \infty$).

The metallic-nanowire-loaded SOI waveguide (MNL SOIW), shown schematically in Fig.1(a), consists of a metal nanowire placed near a SOI substrate, with a low-index, nanometer-scale silica buffer sandwiched between them. The low-index layer offers efficient squeezing of the optical mode within a nanoscale gap region, thus enabling further reduction of the modal loss. Furthermore, similar to the previously studied hybrid waveguides¹⁴⁻¹⁹, the hybridization between the nanowire plasmon and SOI photonic modes can be regulated through tuning the gap size and other structural parameters of the waveguide, and thus allows efficient control of the modal characteristics. The SEM image of a fabricated configuration with a silver nanowire directly placed atop a silicon substrate is shown in Fig.1(b). In the following, the properties of the MNL SOIWs are investigated numerically by solving the Helmholtz equation using the eigenmode solver of a finite element method (FEM) based software COMSOLTM with the scattering boundary condition. Convergence tests are done to ensure that the numerical boundaries and meshing do not interfere with the solutions. The refractive indices of SiO₂, Si, air and Ag at an operating wavelength of 1550 nm are taken as $n_g = n_s = 1.444$, $n_d = 3.476$, $n_c = 1$ and $n_m = 0.1453 + 14.3587i$ ¹⁴, respectively.

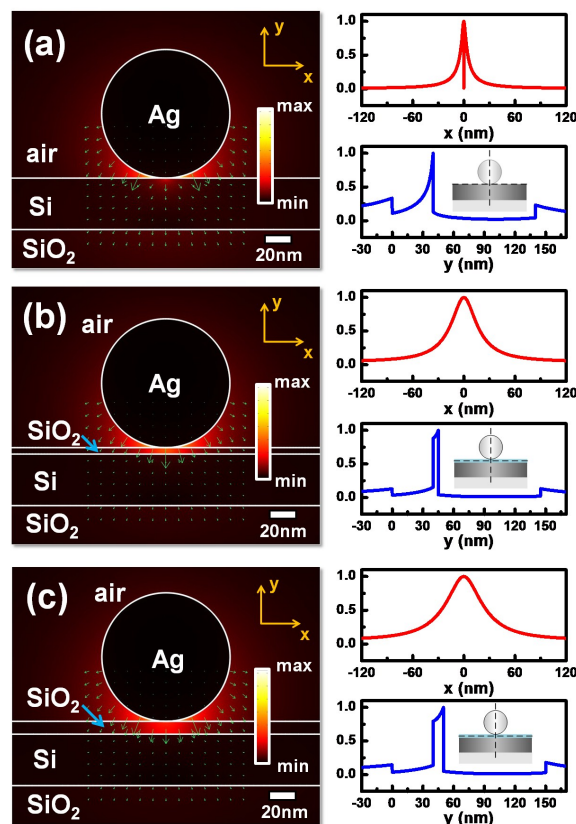


Fig.2 2D electric field distributions and the corresponding 1D normalized field plots of the fundamental hybrid plasmonic modes guided by the MNL SOIWs with different gap sizes. (a) $g = 0$ nm; (b) $g = 5$ nm; (c) $g = 10$ nm. Other geometric parameters of all these waveguides are chosen as: $r = 50$ nm, $t = 40$ nm. The field profiles are taken at the bottom corner of the Ag nanowire for $g = 0$ nm, while at the center of the gap for $g = 5$ nm and 10 nm.

In Fig.2, we plot the electric field distributions of the fundamental plasmonic modes guided by typical MNLSOIWs with different gap sizes. Note that the extreme case of $g = 0$ nm (see Fig.2(a)) corresponds to a nanowire-over-substrate (NWOS) structure¹³, where the silver nanowire stands directly on the silicon waveguide. It is clearly seen that for the configuration with $g = 0$ nm, the field is strongly localized near the bottom of the silver nanowire, resulting in an ultra-small mode area. Introducing a thin silica layer between the nanowire and the silicon waveguide could lead to pronounced field enhancement inside the low-index gap region (see Figs.2(b)-(c)), which is also beneficial for the realization of tight optical confinement. The portion of the mode field confined inside the gap can be further increased through adopting a slightly thicker silica layer. Although the local field enhancement becomes less significant for the larger gap case, the associated modal attenuation reduces correspondingly, leading to extended propagation distances. The evolution of the field profiles and modal properties in Fig.2 reveal that by choosing an appropriate gap size, tight field confinement in conjunction with reasonable propagation distance can be achieved simultaneously by MNLSOIW.

To quantitatively illustrate the waveguide's potential in low-loss subwavelength light transport, we calculate its key modal parameters with the variation of physical dimensions. The properties of the guided plasmon mode are characterized by a complex wave vector, whose parallel component defines the propagating constant with $\beta + i\alpha$. Here, β and α are the phase and attenuation constants, respectively. The real part of the modal effective index is calculated by $n_{\text{eff}} = \text{Re}(N_{\text{eff}}) = \beta/k_0$, where k_0 is the vacuum wavevector. The propagation length is obtained by $L = 1/2\alpha = \lambda/[4\pi\text{Im}(N_{\text{eff}})]$. The normalized mode area is defined as A_{eff}/A_0 , where the effective mode area is calculated using¹⁴

$$A_{\text{eff}} = \iint W(\mathbf{r}) dA / \max(W(\mathbf{r})) \quad (1)$$

In order to accurately account for the energy in the metallic region, the electromagnetic energy density $W(\mathbf{r})$ is defined as:

$$W(\mathbf{r}) = \frac{1}{2} \text{Re} \left\{ \frac{d[\omega \varepsilon(\mathbf{r})]}{d\omega} \right\} |E(\mathbf{r})|^2 + \frac{1}{2} \mu_0 |H(\mathbf{r})|^2 \quad (2)$$

In Eq. (2), $E(\mathbf{r})$ and $H(\mathbf{r})$ are the electric and magnetic fields, $\varepsilon(\mathbf{r})$ is the electric permittivity and μ_0 is the vacuum magnetic permeability. A_0 is the diffraction-limited mode area in free space, which is defined as $\lambda^2/4$. The confinement factor is defined as the ratio of the power inside the considered region to the total power of the waveguide. In order to enable comparisons between the optical performances of different configurations, a figure of merit (FoM), defined as the ratio between the propagation length and the effective mode diameter $2(A_{\text{eff}}/\pi)^{1/2}$, is also calculated.

We start our investigation by studying the effect of the silicon layer on the modal properties of MNLSOIWs with different gap sizes. Figure 3 shows the modal effective index, propagation length, normalized mode area and confinement factor of the fundamental plasmonic mode for different silicon layer's thicknesses when g varies from 0 to 12 nm, where the radius of the silver nanowire is fixed at 50 nm. The gradual thickening of the silica gap layer leads to monotonic behaviors of the effective index, propagation distance and mode area, while resulting in more complicated trends in confinement factors within both the

gap region and the silicon layer. Widening the gap from 0 to 12 nm results in a several-fold enhancement in the traveling distance of the plasmonic mode (up to more than 60 μm), while sacrificing its field confinement capability to a certain extent. Interestingly, deep-subwavelength mode size can be maintained within the considered structural parameter range, along with reasonable power confinement inside both the low-index gap and high-index dielectric layer. The relatively large modal overlap with the low- and high-index dielectric regions are quite beneficial for applications in nanolasers and other active components, which will be shown in our later discussions.

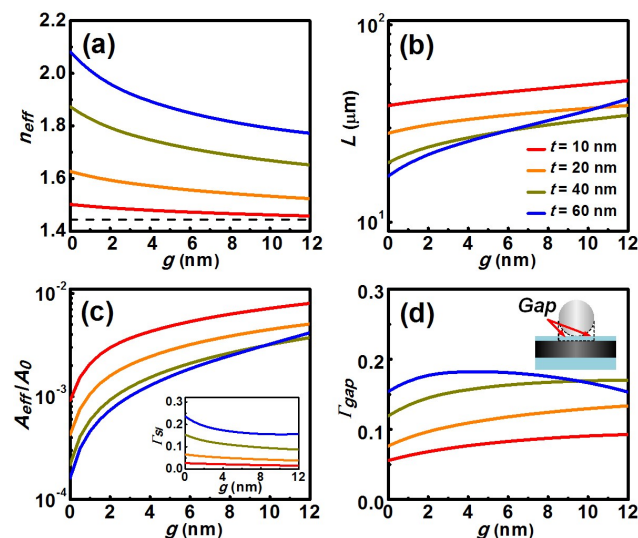


Fig.3 Dependence of the modal properties on the size of the silica gap for different silicon layers ($r = 50$ nm): (a) modal effective index (n_{eff}); (b) propagation length (L); (c) normalized mode area (A_{eff}/A_0), where the inset plots the confinement factor inside the silicon layer (Γ_{Si}); (d) confinement factor in the hybrid gap (Γ_{gap}). Dashed black line in (a) represents the refractive index of the SiO_2 substrate ($n_s = 1.444$). The inset in (d) shows schematically the considered gap region in the study.

We then turn to explore the feasibility of controlling the guiding properties of MNLSOIW by varying the size of the silver nanowire. Since the fundamental plasmonic mode originates from the hybridization of nanowire plasmon and silicon waveguide modes, its modal property shares similarity with that of the pure metallic nanowire mode to a certain degree. In the simulations, the thickness of the Si layer is fixed at 40 nm to ensure low propagation loss, subwavelength mode size and reasonable confinement inside both the low-index gap and high-index dielectric layer. As the nanowire grows larger, decreased field localization, along with gradually extended propagation distance can be observed for MNLSOIWs with different gap sizes. It is seen in Figs.4(b)-(c) that when r varies within the range of 10 to 80 nm, the mode sizes are maintained at the deep-sub-diffraction-limited scale, with A_{eff}/A_0 falling within the range of 10^{-5} – 10^{-2} , while reasonable propagation distances around a few to tens of microns can be achieved simultaneously. Calculations further reveal that the power ratios confined inside both the hybrid gap and the silicon layer experience relatively slight changes with the variation of the nanowire, indicating quite stable optical confinement in both the low- and high-index dielectric regions for waveguides with different metallic nanowires.

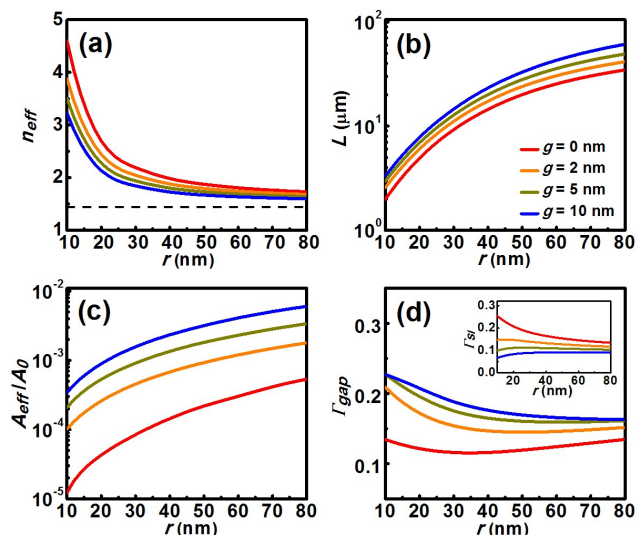


Fig.4 Dependence of the modal properties on the radius of the silver nanowire for different gap sizes ($t = 40$ nm): (a) modal effective index (n_{eff}); (b) propagation length (L); (c) normalized mode area (A_{eff}/A_0); (d) confinement factor in the gap (Γ_{gap}), where the inset plots the confinement factor inside the silicon layer (Γ_{Si}). Dashed black line in (a) corresponds to the refractive index of the SiO_2 substrate ($n_s=1.444$).

To benchmark the optical performance of the considered MNLSOIW, comparisons with a bare metallic nanowire in an air cladding and a conventional hybrid plasmonic waveguide (HPW) are made by performing 2D parametric plots of normalized mode area versus normalized propagation length. Detailed results in Fig.5 illustrate that for similar propagation distances, the mode area of MNLSOIW can be 1~2 orders of magnitude smaller than that of the metal nanowire waveguide (MNW) in air, while being 1 order of magnitude smaller as compared to the conventional HPW. Calculations of FoMs further confirm the superior guiding properties of metallic-nanowire-loaded SOI structures. The FoMs of MNLSOWs can exceed the order of 10^3 , revealing significant enhancements over the conventional MNWs, HPWs and many other subwavelength plasmonic waveguides²¹⁻²³ under comparable conditions (see S1 of the supplementary information for details).

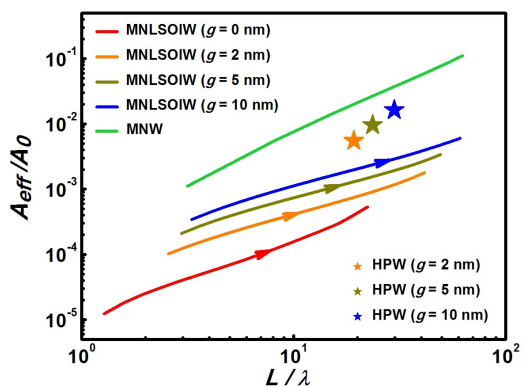


Fig. 5 Parametric plots of normalized mode area (A_{eff}/A_0) versus normalized propagation length (L/λ) for MNLSOIWs, MNWs and HPWs. The curves for MNLSOIWs are obtained by reploting the results in Figs.4 (b)-(c). A trajectory corresponds to a range of silver nanowire radius: $r = [10, 80]$ nm. Arrows indicate increasing the size of the nanowire. For MNWs, the radii are also varied within the range of 10 nm to 80 nm. For HPWs, the geometries and dimensions are chosen

according to¹⁴, which are composed of 200-nm diameter silicon nanowires embedded in silica near planar silver surfaces. The refractive indices of the materials for both MNWs and HPWs are the same as those of the studied MNLSOIWs to allow fair comparisons.

3. Metallic-nanowire-loaded SOI waveguides for practical applications : Investigations on waveguide crosstalk and gain-assisted light guiding

For practical implementations of MNLSOIW, one of the most important issues to be addressed is the efficient launching of its guided mode. Owing to the hybrid nature of the fundamental plasmonic mode supported by MNLSOIW, excitation strategies that are similar to the conventional^{1, 24} and modified metal nanowire waveguides^{13, 25, 26}, such as near-field coupling techniques^{27, 28}, far-field illumination methods^{6, 29, 30} and other ways that can overcome the momentum mismatch, can be adopted. By performing full-wave 3D FEM simulations, here we numerically demonstrate the excitation of the fundamental plasmonic mode guided by MNLSOIW. The schematic of the excitation setup is shown in Fig.6 (a), where a paraxial Gaussian beam is focused normally onto the left terminus of the silver nanowire²⁴. Simulation results shown in Figs.6 (b)-(d) clearly reveal that when the incident polarization of the beam is parallel to the silver nanowire (i.e. along the z axis), a plasmonic mode featuring tight field localization near both the nanowire and the gap region can be effectively launched and propagates along the structure with moderate attenuation, which confirms the feasibility of MNLSOI mode excitation using focused laser beams.

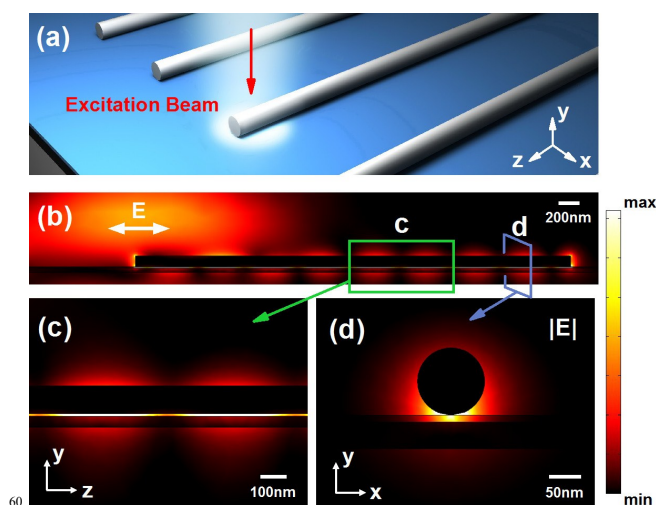


Fig. 6 Excitation of the fundamental plasmonic mode guided by MNLSOIW. (a) 3D schematic of the excitation setup. In the simulations, the length of the silver nanowire is assumed to be 4 μm . The structural parameters for the cross-section of the configuration are: $r = 50$ nm, $t = 40$ nm, $g = 10$ nm; (b)-(c) 2D transmitted electric field plots in the y - z plane ($x = 0$); (d) 2D electric field profile at the cross-section of the structure (x - y plane).

A key parameter to evaluate the potential of plasmonic waveguides for compact photonic integrations is the crosstalk between adjacent structures, which can be gauged through calculating the coupling lengths of two closely spaced waveguides^{31, 32}. Here we look into the crosstalk property of the MNLSOIW, and compare it with that of the conventional MNW

in an air cladding. In Fig.7 (a), we show schematically the configuration of a coupling system that comprises two horizontally parallel MNLISOIWs with a center-to-center separation of S . The major components of the electric fields for the symmetric and anti-symmetric super-modes in a typical MNLISOIW-based system, as plotted in Fig.7 (b), illustrate relatively weak modal overlap between neighboring structures, which is beneficial for the realization of large coupling length and low waveguide crosstalk. Fig.7 (c) reveals the calculated normalized coupling lengths (L_c/L) for various waveguide separations, where the coupling length (L_c) between neighboring MNLISOIWs/MNWs are obtained based on the coupled mode theory³³:

$$L_c = \pi / |k_s - k_a| \quad (3)$$

In Eq.(3), k_s and k_a are the wavenumbers of the symmetric and anti-symmetric modes of two coupled waveguides, respectively. As clearly seen in Fig.7 (c), owing to the high optical confinement of MNLISOIWs, their normalized coupling lengths are significantly larger than that of the conventional MNW with the same metallic nanowire, which suggests clear reductions in crosstalk for nearby waveguiding structures. Furthermore, our calculations reveal that MNLISOIWs also demonstrate relatively good propagation characteristics through 90° bends (See S2 of the supplementary material). The low crosstalk and nice bending properties of MNLISOIWs could facilitate potential applications in optical interconnects and enable the implementations of numerous ultra-compact photonic devices.

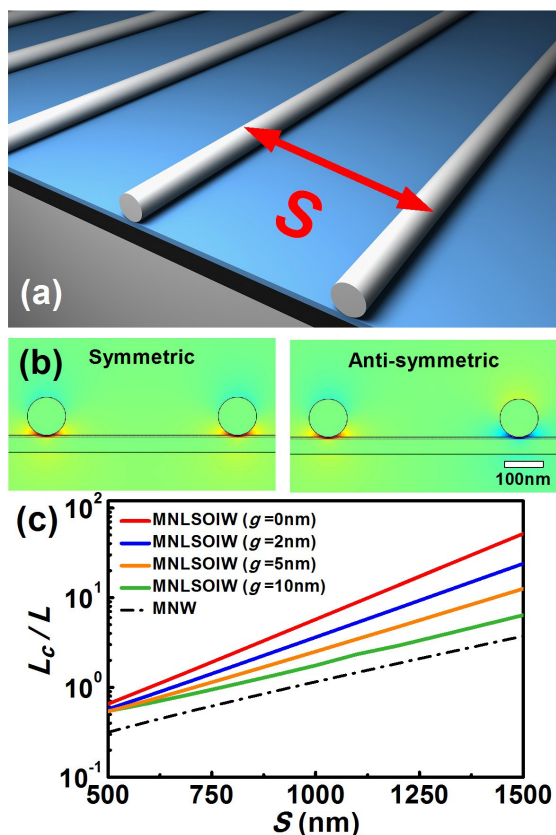


Fig. 7 Studies on the crosstalk between adjacent MNLISOIWs. (a) Schematic of the coupling system containing horizontally parallel MNLISOIWs with a center-to-center separation of S ; (b) E_v field distributions of the symmetric and anti-symmetric plasmonic modes in the MNLISOIW-based coupling systems ($r = 50$ nm, $t = 40$ nm, $g = 5$ nm, $S =$

500 nm); (c) Dependence of normalized coupling length (L_c/L) on the separation (S) between two MNLISOIWs ($r = 50$ nm, $t = 40$ nm). The result of a bare metallic nanowire waveguide in an air cladding ($r = 50$ nm) is also plotted to enable comparisons between their performances.

Although our previous studies indicate that low-loss light propagation can potentially be enabled by MNLISOIW, the attenuation of its guided mode still exists owing to the damping of electromagnetic waves in the metallic nanowire. One of the most effective approaches to overcome this challenge is by implementing loss compensation strategies, which can be achieved through incorporating gain media into the dielectric layers of the waveguide. For the currently studied MNLISOIW, the pump light may be introduced through back-side illumination^{34, 35}. Such gain-assisted light guiding can enable complete compensation of the modal loss as long as appropriate gain is provided, thereby leading to loss-less transport of the plasmonic mode. By assuming that gain is introduced in the high-index silicon layer or the low-index silica layer just beneath the silver nanowire, we conduct detailed investigations on the loss compensation in the proposed metallic-nanowire-loaded waveguides. Here we first look into the gain enhancements that could be enabled by these guiding configurations. The enhancement in gain is evaluated by calculating the ratio $\partial g_m / \partial g_{\text{silicon}}$ ($\partial g_m / \partial g_{\text{silica}}$), where g_m is the gain of the guided plasmonic mode and g_{silicon} (g_{silica}) represents the gain of the bulk material (i.e. silicon/silica). Note that the gain coefficients of the plasmon mode and the bulk material are written in terms of the imaginary part of the modal effective index or refractive index, i.e. $2 \times 2\pi/\lambda \times \text{Im}(N)$ ³⁶. As shown in Figs. 8 (a)-(b), $\partial g_m / \partial g_{\text{silica}}$ experiences more significant changes with the variation of the silver nanowire than $\partial g_m / \partial g_{\text{silicon}}$. For waveguides with small nanowires and relatively large gaps, the enhancement ratios in silica cases approach 1. While our calculations indicate that such ratios can even exceed 1 through structural parameter tuning, e.g. by further enlarging the gap, minimizing the nanowire size and/or increasing the thickness of the silicon layer. The large gain enhancement ratios under these circumstances also indicate that more gain can be achievable in the guided structure than that would be possible in bulk media, which is largely attributed to the combined effects of the high power confinement inside the low/high-index region and the significant improvement of the group index over the bulk refractive index, similar to that observed in high-index contrast silicon slot waveguides³⁶. Such unique features also potentially facilitate the implementation of compensating the modal loss of MNLISOIW. To demonstrate the feasibility of loss compensation, we show the loss or gain of the plasmonic mode supported by a specific MNLISOIW when gain in the silicon/silica layer gradually increases. In the calculations, the radius of the metallic nanowire is fixed at 50 nm to ensure relatively large confinement factor and small modal loss. As seen in Figs.8 (c)-(d), the loss or gain increases linearly as the gain in bulk medium increases, illustrating that the modal loss can be reduced dramatically as long as moderate gain is introduced. When gain is large enough, the attenuation of the mode can be fully compensated, which is revealed by the crossing points of the solid and dashed black lines in Figs.8 (c)-(d). At these critical conditions, the imaginary part of the modal effective index equals zero, enabling lossless propagation of the mode at the nanoscale.

Such a critical material gain for lossless light transport, which is subject to the tradeoff between modal loss/gain and field confinement, may be further reduced by adjusting geometric parameters.

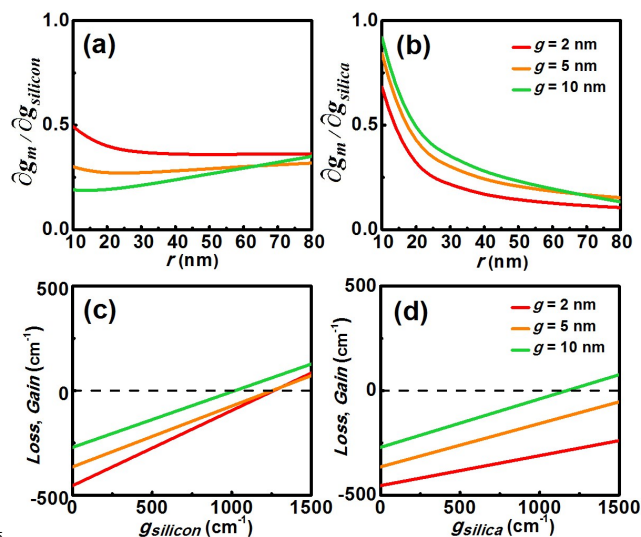


Fig. 8 Loss compensation in MNLISOIW structures ($r = 50$ nm, $t = 60$ nm): (a)-(b) Gain enhancement ratios for the fundamental plasmonic modes supported by various geometries when gain is introduced in the silicon layer ($\partial g_m / \partial g_{\text{silicon}}$) or the silica layer ($\partial g_m / \partial g_{\text{silica}}$). (c)-(d) Dependence of the modal gain/loss on the introduced gain coefficient in the silicon/silica layer.

For the studied MNLISOIW in the previous section, an alternative structure is a dielectric-coated silver nanowire on a SOI substrate, as shown schematically in Fig.9 (a). Despite its slightly increased modal attenuation, this waveguide enables better confinement inside the silica gap layer and requires less material gain for loss compensation applications, which is also a marked difference from the previously investigated MNLISOIW. Remarkably, both types of MNLISOIW structures are technologically feasible from a practical point of view³⁷⁻³⁹, thus allowing further implementations of numerous compact photonic devices based on these nanowire integrated SOI configurations. Moreover, the enhanced guiding properties of MNLISOIW structures over traditional metallic nanowire waveguides also facilitate a wide variety of potential applications, including those in (bio) chemical sensing, opto-mechanics and quantum photonics. Here it is worth mentioning that in addition to the circular nanowire studied here, metallic configurations with triangular¹⁷, rectangular^{40, 41}, pentagonal³⁹ or other similar cross-sectional shapes⁴² can also be adopted to build high-performance MNLISOI structures. Furthermore, the proposed waveguide concept can be extended into many other metal-dielectric nanostructures as well, such as metal-insulator-metal and insulator-metal-insulator structures, which may result in improved field confinement or reduced modal attenuation as compared to the MNLISOIW structures studied here (see S3 in the supplementary information for details).

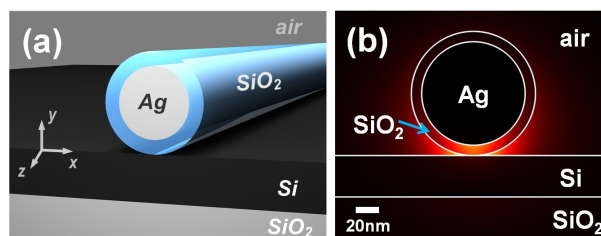


Fig. 9 An alternative MNLISOI configuration consisting of a silica-coated silver nanowire on a SOI substrate with an air cladding. (a) 3D schematic of the waveguide structure; (b) Electric field profile of the fundamental plasmonic mode in a typical waveguide, whose structural parameters are: $r = 50$ nm, $t = 40$ nm and $g = 10$ nm. Here, g denotes the thickness of the silica coating, which also defines the size of the gap between the silver nanowire and the silicon waveguide.

4. Conclusion

In conclusion, we have shown that high-performance plasmon waveguiding can be enabled by integrating SOI substrates with metallic nanowires. The low-index buffer layer sandwiched between them greatly facilitates the hybridization of dielectric and plasmonic modes, thus allowing efficient light transport on the nanoscale with reasonable propagation distance ranging from tens to hundreds of microns at telecommunication wavelength. Studies on mode excitation, waveguide crosstalk and gain-assisted light propagation further reveal the potential capabilities of SOI-integrated nanowire structures in building both passive and active components. Due to their promising optical properties, the studied metallic-nanowire-loaded SOI waveguides can be useful additions to the expanding family of nanowire and hybrid plasmonic structures, opening exciting venues in a variety of application fields.

60 Acknowledgements

This work was supported by the National Key Basic Research Program of China (Grant No. 2013CB328704), the National Natural Science Foundation of China (Grants No. 11121091, No. 91221304, No. 11134001 and No. 11304004), and the Postdoctoral Science Foundation of China (2014T70012 and 2013M530462). The authors would like to acknowledge Dr. Pengfei Yang at Institute of Physics, Chinese Academy of Sciences, Prof. Zheng Zheng at Beihang University, Prof. Hong Yang, Prof. Xiaoyong Hu, Prof. Ying Gu, Prof. Yunfeng Xiao, Prof. Jianjun Chen, Prof. Rui Zhu, Prof. Guowei Lu, Dr. Cuicui Lu, Dr. Youling Chen, Dr. Chengwei Sun, Dr. Qin Hu, Dr. Xiang Zhang, Dr. Zhen Chai and Dr. Donghai Li at Peking University for useful discussions.

75 Notes and references

^a State Key Laboratory for Mesoscopic Physics, Department of Physics, Peking University, Beijing 100871, P. R. China

^b Collaborative Innovation Center of Quantum Matter, Beijing 100871, China

E-mail: qhgong@pku.edu.cn

Electronic supplementary information (ESI) available: S1: FoMs of MNLISOIW and other typical plasmonic waveguides; S2: Bending properties of MNLISOIW structures; S3: Alternative configurations. See DOI: 10.1039/c0nr00135j

1. H. Wei and H. X. Xu, *Nanophotonics*, 2012, **1**, 155-169.
2. J. Takahara, S. Yamagishi, H. Taki, A. Morimoto and T. Kobayashi,
5 *Opt. Lett.*, 1997, **22**, 475-477.
3. Z. H. Han and S. I. Bozhevolnyi, *Rep. Prog. Phys.*, 2013, **76**, 016402.
4. X. Guo, M. Qiu, J. Bao, B. J. Wiley, Q. Yang, X. Zhang, Y. Ma, H. Yu
and L. Tong, *Nano Lett.*, 2009, **9**, 4515-4519.
5. H. Wei, Z. X. Wang, X. R. Tian, M. Kall and H. X. Xu, *Nature*
10 *Communications*, 2011, **2**.
6. H. Ditlbacher, A. Hohenau, D. Wagner, U. Kreibig, M. Rogers, F.
Hofer, F. R. Aussenegg and J. R. Krenn, *Phys. Rev. Lett.*, 2005, **95**,
257403.
7. X. Q. Wu, Y. Xiao, C. Meng, X. N. Zhang, S. L. Yu, Y. P. Wang, C. X.
15 Yang, X. Guo, C. Z. Ning and L. M. Tong, *Nano Lett.*, 2013, **13**, 5654-
5659.
8. C. L. Zou, F. W. Sun, Y. F. Xiao, C. H. Dong, X. D. Chen, J. M. Cui,
Q. Gong, Z. F. Han and G. C. Guo, *Appl. Phys. Lett.*, 2010, **97**, 183102.
9. Z. Li, K. Bao, Y. Fang, Z. Guan, N. J. Halas, P. Nordlander and H. Xu,
20 *Phys. Rev. B*, 2010, **82**, 241402(R).
10. Y. P. Wang, Y. G. Ma, X. Guo and L. M. Tong, *Opt. Express*, 2012,
20, 19006-19015.
11. Q. Li and M. Qiu, *Opt. Express*, 2013, **21**, 8587-8595.
12. W. Wei, X. Zhang, H. Yu, Y. Q. Huang and X. M. Ren, *Photon. Nano.*
25 *Fund. Appl.*, 2013, **11**, 279-287.
13. S. P. Zhang and H. X. Xu, *Acs Nano*, 2012, **6**, 8128-8135.
14. R. F. Oulton, V. J. Sorger, D. A. Genov, D. F. P. Pile and X. Zhang,
Nat. Photon., 2008, **2**, 496-500.
15. D. X. Dai and S. L. He, *Opt. Express*, 2009, **17**, 16646-16653.
- 30 16. M. Z. Alam, J. S. Aitchison and M. Mojahedi, *Laser Photonics Rev.*,
2014, **8**, 394-408.
17. Y. S. Bian and Q. H. Gong, *Laser Photonics Rev.*, 2014 **8**, 549-561.
18. Y. Liang, W. Wu, J. Huang and X. Huang, *Nanoscale*, 2014, **6**, 12360-
12365.
- 35 19. M. M. Jiang, H. Y. Chen, C. X. Shan and D. Z. Shen, *Phys. Chem.*
Chem. Phys., 2014, **16**, 16233-16240.
20. R. Buckley and P. Berini, *Opt. Express*, 2007, **15**, 12174-12182.
21. S. I. Bozhevolnyi, V. S. Volkov, E. Devaux, J. Y. Laluet and T. W.
Ebbesen, *Nature*, 2006, **440**, 508-511.
- 40 22. L. Liu, Z. Han and S. He, *Opt. Express*, 2005, **13**, 6645-6650.
23. T. Holmgaard and S. I. Bozhevolnyi, *Phys. Rev. B*, 2007, **75**, 245405.
24. S. P. Zhang, H. Wei, K. Bao, U. Hakanson, N. J. Halas, P. Nordlander
and H. X. Xu, *Phys. Rev. Lett.*, 2011, **107**, 096801.
25. Y. S. Bian and Q. H. Gong, *IEEE J. of Quantum Electron.*, 2013, **49**,
45 870-876.
26. Y. S. Bian, Z. Zheng, P. F. Yang, J. Xiao, G. J. Wang, L. Liu, J. S. Liu,
J. S. Zhu and T. Zhou, *IEEE J. Sel. Top. Quantum Electron.*, 2014, **20**,
8100108.
27. Y. G. Ma, X. Y. Li, H. K. Yu, L. M. Tong, Y. Gu and Q. H. Gong, *Opt.*
50 *Lett.*, 2010, **35**, 1160-1162.
28. W. Wang, Q. Yang, F. Fan, H. Xu and Z. L. Wang, *Nano Lett.*, 2011,
11, 1603-1608.
29. A. W. Sanders, D. A. Routenberg, B. J. Wiley, Y. N. Xia, E. R.
Dufresne and M. A. Reed, *Nano Lett.*, 2006, **6**, 1822-1826.
- 55 30. M. W. Knight, N. K. Grady, R. Bardhan, F. Hao, P. Nordlander and N.
J. Halas, *Nano Lett.*, 2007, **7**, 2346-2350.
31. J. A. Conway, S. Sahni and T. Szkopek, *Opt. Express*, 2007, **15**, 4474-
4484.
32. G. Veronis and S. H. Fan, *Opt. Express*, 2008, **16**, 2129-2140.
- 60 33. W. P. Huang, *J. Opt. Soc. Am. A*, 1994, **11**, 963-983.
34. J. Zhang, L. Cai, W. Bai, Y. Xu and G. Song, *Opt. Lett.*, 2011, **36**,
2312-2314.
35. D. Dai, Y. Shi, S. He, L. Wosinski and L. Thylen, *Opt. Express*, 2011,
19, 12925-12936.
- 65 36. J. T. Robinson, K. Preston, O. Painter and M. Lipson, *Opt. Express*,
2008, **16**, 16659-16669.
37. Y. D. Yin, Y. Lu, Y. G. Sun and Y. N. Xia, *Nano Lett.*, 2002, **2**, 427-
430.
38. J. A. Sioss, R. L. Stoermer, M. Y. Sha and C. D. Keating, *Langmuir*,
70 2007, **23**, 11334-11341.
39. H. Wei, S. P. Zhang, X. R. Tian and H. X. Xu, *Proc. Natl Acad. Sci.*
USA, 2013, **110**, 4494-4499.
40. Y. S. Bian, Z. Zheng, X. Zhao, L. Liu, Y. L. Su, J. Xiao, J. S. Liu, J. S.
Zhu and T. Zhou, *J. Lightwave Technol.*, 2013, **31**, 1973-1979.
- 75 41. L. J. E. Anderson, Y. R. Zhen, C. M. Payne, P. Nordlander and J. H.
Hafner, *Nano Lett.*, 2013, **13**, 6256-6261.
42. S. Nauert, A. Paul, Y. R. Zhen, D. Solis, L. Vigderman, W. S. Chang,
E. R. Zubarev, P. Nordlander and S. Link, *Acs Nano*, 2014, **8**, 572-580.
- 80